Synthesis of nano- and micro-scale topographies by combining colloidal lithography and glancing angle deposition (GLAD)

Dolatshahi-Pirouz, Alireza; Kolind, Kristian; Pennisi, Cristian Pablo; Duroux, Meg; Zachar, Vladimir; Foss, Morten; Besenbacher, Flemming

Published in:
Advanced Engineering Materials

DOI (link to publication from Publisher):
10.1002/adem.201400044

Publication date:
2015

Document Version
Publisher's PDF, also known as Version of record

ADVANCED ENGINEERING MATERIALS

COMMUNICATION

DOI: 10.1002/adem.201400044

Synthesis of Nano- and Micro-Scale Topographies by Combining Colloidal Lithography and Glancing Angle Deposition (GLAD)**

By *Alireza Dolatshahi-Pirouz,* Kristian Kolind, Cristian Pablo Pennisi, Meg Duroux, Vladimir Zachar, Morten Foss* and *Flemming Besenbacher*

A great challenge when developing materials for application in biomedical engineering is to design interfaces that ultimately can control the interaction between cells and the biomaterial.[1–3] Previously, nanoscale surface topographies have been reported to influence biological processes such as protein adsorption,[4–6] cellular responses,[7–9] and blood clotting,[10] making it an important factor in developing biomaterials for medical applications. Inspired by the native microenvironment of cells, which contain dual-scale topographies in the micro and nanoscale, different methods have been proposed to design such native-like topographies for optimization of biomaterials.[11–13] However, to date none of the methods have offered the possibility to change the nanoscale roughness on sub-micrometer topographies in a well-controlled manner. Surfaces with a well-controlled roughness for various applications can be manufactured through glancing angle deposition (GLAD).[14–20] During GLAD, a flux of vaporized particles impinge at the substrate at an oblique angle of incidence causing regionalized shadowing and thereby an enhanced surface roughening.[21,22] Colloidal surface patterning on the other hand can generate ordered submicron structures with a well-defined periodicity.[22]

Here, we present a method by means of which we can synthesize unique platinum surfaces with controlled micro- and nano-scale topographies through a combination of (GLAD) and colloidal surface patterning.[23–27] Platinum was used since it offers a good biocompatibility and constitutes an integral part in various implantable electrodes. Like most implants, electrodes trigger a foreign body response, which ultimately results in the formation of a nonconductive capsule that compromises their functionality.[28] This capsule consist of fibroblasts or glial cells depending on whether the electrode is implanted in the peripheral or central nervous system, respectively. The potential biomedical application of our surfaces was therefore investigated by studying the interaction of human skin-derived fibroblasts and glial cells with the surfaces in terms of cell attachment, spreading, and morphology. Combining the GLAD technique with the colloidal surface patterning technique, results in the fabrication of well-defined and separated topographies with a unique micro- and nanoscale roughness.[23–27] More specifically, bare silicon wafers were pre-coated with 110 nm colloidal particles followed by a 5 nm platinum (Pt) sputter coating to assure chemical homogeneity of the surfaces prior to the GLAD process, which was performed at an oblique angle of 5°. The nano-particles were subsequently melted by heating the samples to 160 °C for approximately 1 h before being sputter coated with 25 nm of Pt (Figure 1A). The heat treatment only reduced the size of the nano-particles by 20–25 nm when compared to the size prior to heating and sputtering (see Supporting Information Figure S1).

The surface morphology of the fabricated surfaces was examined by atomic force microscopy (AFM; Figure 1B–E), which revealed stochastically dispersed nano-features on the flat-reference surfaces and on the submicron islands. From AFM line-scans, we find that the nanoscale features increased in size as the amount of deposited Pt increased. Likewise, examination of the fabricated surfaces with planar- and cross-sectional scanning electron microscopy

[*] *A. Dolatshahi-Pirouz, K. Kolind, M. Foss, F. Besenbacher*
Interdisciplinary Nanoscience Center (iNANO), Aarhus University, DK-8000 Aarhus C, Denmark
E-mail: alirezadolatshahipirouz@gmail.com
C. P. Pennisi, M. Duroux, V. Zachar
Laboratory for Stem Cell Research, Aalborg University, DK-9220 Aalborg, Denmark
M. Duroux
Laboratory for Cancer Biology Biomedicine, Aalborg University, Fredrik Bajers Vej 3 B, Aalborg Ost, DK 9220, Denmark
F. Besenbacher
Department of Physics and Astronomy, Aarhus University, DK-8000 Aarhus C, Denmark
A. Dolatshahi-Pirouz and K. Kolind contributed equally to this work.

[**] *We gratefully thank Coloplast A/S for financial support, for providing the human fibroblasts for this study and for lab facilities during seeding and culturing of cells, and we thank the Interdisciplinary Nanoscience Center, Aarhus University, Denmark, for financial support (Supporting Information is available online from Wiley Online Library or from the author). Note: Reference 2 was corrected after initial online publication.*

ADVANCED ENGINEERING MATERIALS

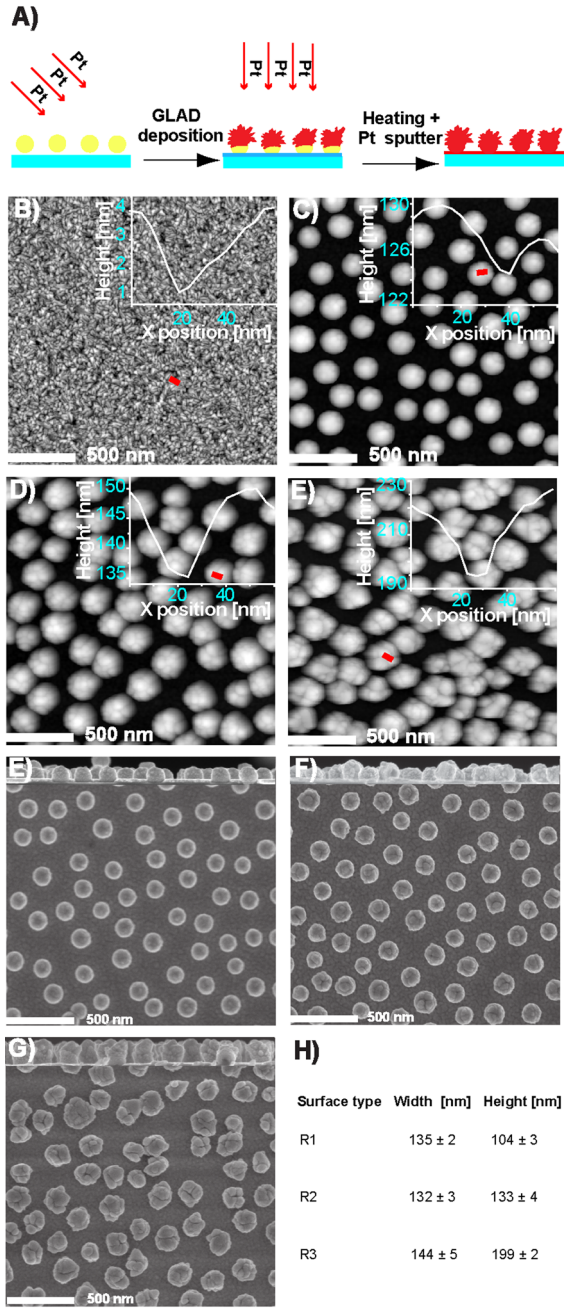

Fig. 1. (A) Illustration of the fabrication process. (B) AFM images of the flat control, (C) surface R1 (1.6×10^{-5} (g cm^{-2})) (D) R2 (3.2×10^{-5} (g cm^{-2})) and (E) R3 (6.4×10^{-5} (g cm^{-2})). The red lines mark the position were the line-scans in the upper right corner of the AFM images were taken. (F) Plan-view and cross-section SEM images of surface R1, (G) R2 and (H) R3. (I) Table showing the mean widths and heights of the submicron islands ± standard error of the mean. For each surface type the width and height of 15 islands were measured.

(SEM; Figure 1F–H) revealed well-separated islands along with a thin Pt layer of approximately 20–25 nm, confirming the successful sputtering of Pt onto the surfaces (Figure 1F–H). Furthermore, a detailed analysis of the width and characteristic heights of the individual submicron islands from cross-sectional SEM images showed a similar island width on the respective surfaces, while the maximum height of the islands was observed to increase as the amount of deposited Pt was increased (Figure 1I). The AFM and SEM results thus confirmed that by combining GLAD and colloidal patterning, it is possible to design and synthesize surfaces with well-defined micro- and nano-scale surface topographies.

To study the cellular response of the developed surfaces for their potential use as biomaterials, fibroblast and glial cells were seeded on the surfaces and allowed to attach and spread for 24 h. Determination of the cell density was performed by automatic counting of DAPI stained cell nuclei (Figure 3B). Likewise, an estimate of cell attachment was performed by a qualitative analysis of positively stained vinculin, a protein involved in the formation of focal contacts (Figure 2). Finally, cell spreading was determined by measuring the area of the cells actin stained images and based on this the degree of cell roundness and elongation was calculated (Figure 3C–E). From Figure 3B, significant cell density differences were observed between the control and surfaces R1 and R2 for the fibroblasts and between the control and all the structured surfaces for the glial cells. Among the micro- and nano-structured surfaces surface R2 had a significantly ($p < 0.05$) lower fibroblast cell density compared to R3. Likewise, glial cells had a significantly lower cell density on surface R2 compared to both R1 ($p < 0.01$) and R3 ($p < 0.001$), while no differences were found between R1 and R3. In an analysis of the cell cytoskeleton and the formation of focal adhesion contacts large differences were observed between the structured and the control surfaces. The cytoskeleton of both fibroblast and glial cells on the control surfaces were well spread and contained well-defined actin stress fibers, while the cytoskeleton on the rough surfaces appeared less organized and more diffuse (Figure 2). Also, on the control surfaces fibroblasts had more well defined dash-like vinculin spots (typical of mature focal adhesions) compared to the dot-like (transient) vinculin spots found in fibroblasts cultured on the structured surfaces.[29] The state of the actin cytoskeleton and the morphology of the focal adhesion sites could likely influence subsequent cellular behavior such as the cell proliferation.[30–32] This is however not the main focus here and will be explored further in a subsequent project.

In several studies, the morphology of cells on surfaces in different cellular states[33–36] has been investigated and it is demonstrated that a close correlation exits between the cell morphology and cell function. It is generally accepted that a small, round cell shape is typically indicative of a cell entering apoptosis,[33,37] whereas a well-spread polygonal cell shape is most often quantified as being in a viable, functional state.[33,35] It is possible to quantify cell shape by measuring cell area and calculating the degree of elongation and roundness by means of imaging software packages. From such a quantitative analysis our study revealed that the total area of both fibroblasts and glial cells was significantly larger on the control surfaces as compared to the micro- and nano-structured surfaces (Figure 3C). With regards to cell elongation, it was found that the glial cells were significantly less elongated on the

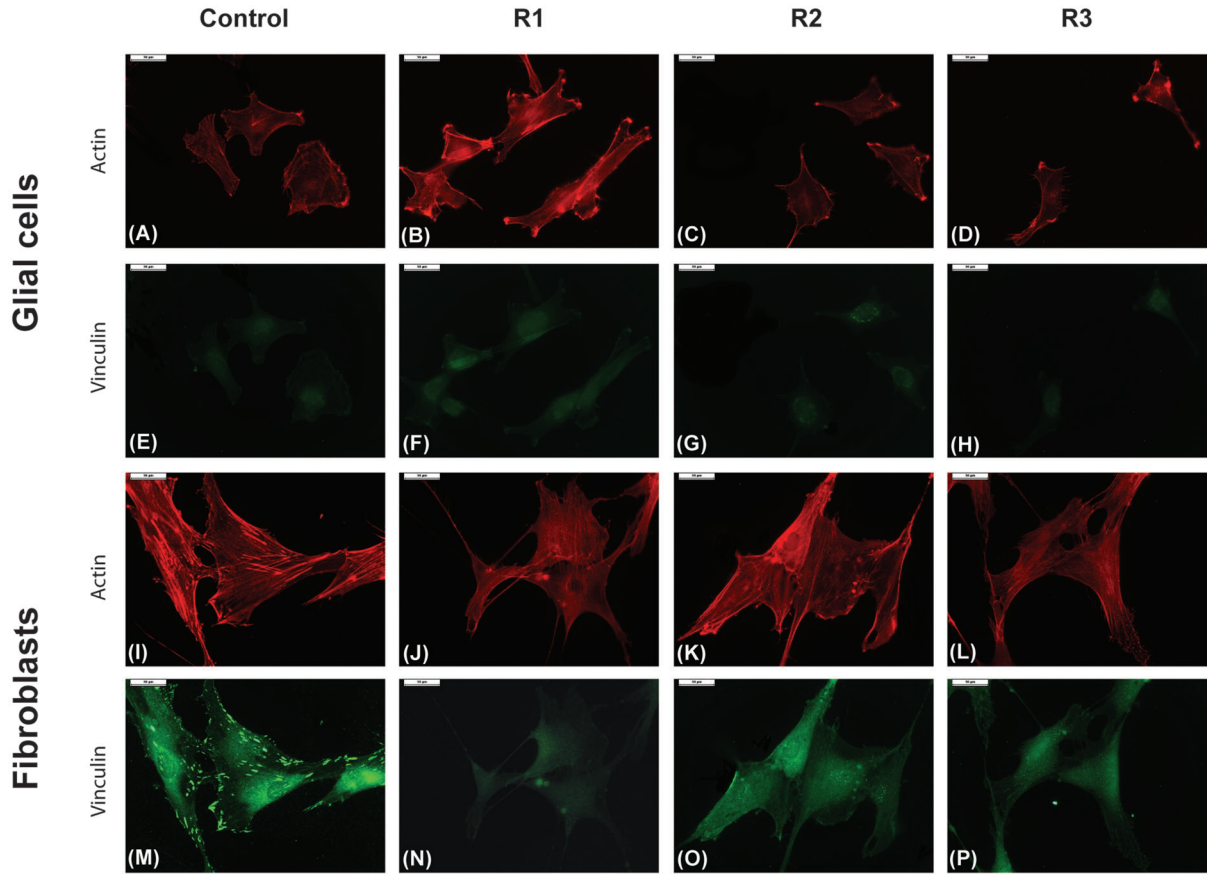

Fig. 2. Representative immunostaining images of glial cells (A–H) and fibroblasts (I–P) on the different surfaces. (A–D) and (I,J) display the actin cytoskeleton, while (E–H) and (M–P) display the vinculin focal adhesions. Scale bar = 30 μm.

control surface as compared to cells on the structured surfaces, while no differences were observed for fibroblasts (Figure 3D). Furthermore, cell roundness of both glial cells and fibroblasts was significantly ($p < 0.001$) lower on the control surfaces compared to the structured surfaces. Also, the roundness value of fibroblasts on surface R1 was significantly ($p < 0.001$) higher than for cells on surface R2.

In Figure 4, we have depicted the roundness values versus the cell area in order to explore any correlation between the two parameters. It was found that a large scatter existed for both cell types on all the studied surfaces indicating that the cells were primarily in a non-round and well-spread state. However, from a detailed analysis of the scatter plots some differences in the distribution patterns were revealed between the fibroblasts and glial cells and among the different surfaces cultured with the same cell type. As such, the scatter observed for fibroblasts was similar on all the surfaces (Figure 4A), but significantly different from the more narrow scatter distribution observed for the glial cells. For the different surfaces cultured with glial cells, it was also found that for surface type R3 the cell roundness values declined as the cell area increased beyond approximately 1500 μm^2 (indicated by vertical line in Figure 4B), while this decrease in cell roundness did not occur before a larger cell area of around 2000 μm^2 for glial cells on the control surface. Thus, we suspect that the individual micro- and nano-structured surfaces may have a larger impact on glial cell morphology than initially anticipated from Figure 3E.

In summary, we have developed an interesting scheme to fabricate surfaces with unique micro- and nano-scale topographies synthesized through colloidal surface patterning and GLAD. By changing the amount of deposited material, we were able to control the surface nano-roughness of the submicron islands in a well-controlled manner. The cellular response of these substrates were investigated in cell adhesion studies with fibroblasts and glial cells, from which it was observed that the structured surfaces influence the initial cell attachment, spreading, cytoskeletal organization and cell morphology. Likewise, it has been demonstrated that the characteristic sizes of the nano-scale features influence glial cell adhesion and the morphology of both cell types. We thus conclude that the proposed GLAD and colloidal surface patterning is a promising new method for designing surfaces with specific micro- and nano-scale topography to control the initial response between cells and surfaces. We envision, that the proposed method may prove as a very useful surface engineering tool in the areas of tissue engineering and biomaterials science.

ADVANCED ENGINEERING MATERIALS

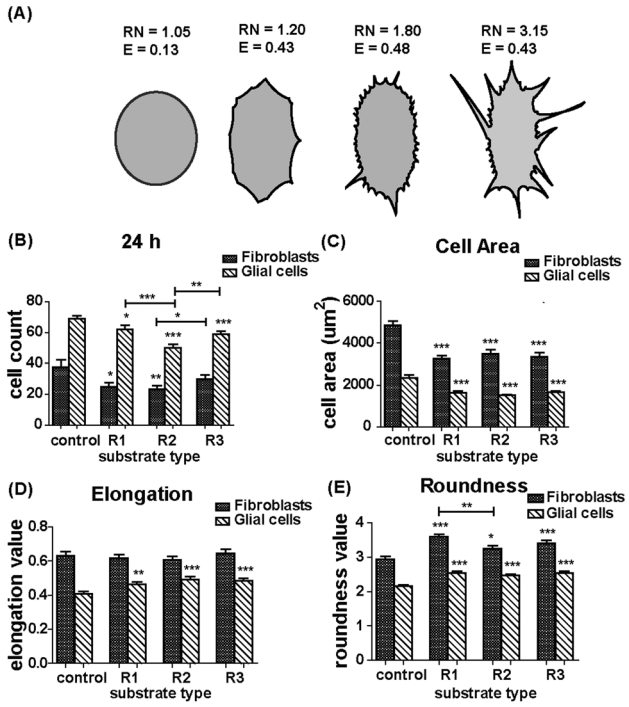

*Fig. 3. (A) Illustration showing roundness and elongation values for cells with different morphologies (B) cell density, (C) area, (D) elongation, and (E) roundness values on the respective surfaces. Significant differences between the individual groups and the control, calculated based on the Students t-test, are marked with *($p < 0.05$), **($p < 0.01$), and ***($p < 0.001$), respectively.*

1. Experimental

1.1. Surface Fabrication

Colloidal particles were deposited onto silicon wafers via electrostatic self-assembly. In brief, silicon wafers (Si-Mat, Germany) were pre-coated with a triple layer precursor film to make the surface positively charged at neutral pH by coating the substrates with: (i) 2% (by weight) poly(diallydimethylammonium) chloride (PDDA, MW 200 000–350 000, Sigma–Aldrich, Denmark), 30 s rinse in milliQ (MQ) water and drying with nitrogen; (ii) 2% (by weight) poly(sodium 4-styrenesulfonate) (PSS, MW 70 000, Sigma–Aldrich, Denmark), 30 s rinse in MQ water and drying with nitrogen; (iii) 5% (by weight) aluminum chloride hydroxide (ACH, chlorohydrol, Reheis, Eire), 30 s in MQ water and drying with nitrogen. Negatively charged latex particles with a diameter of 110 nm (Invitrogen, US) diluted to a concentration of 0.4% (by weight) was subsequently adsorbed onto the charged substrates from solution by electrostatic interactions. The adsorption lasted for 2 min and the substrates were afterward rinsed in MQ water for 1 min before drying with nitrogen. The resultant particle layers were short range ordered arrays of separated particles with surface coverage at $22.7 \pm 1.4\%$ as determined by ImageJ. Prior to the Pt GLAD step the surfaces pre-templated with latex particles were coated at room temperature with 5 nm gold by e-gun evaporation at 90°. The gold deposition step assured that the subsequent GLAD Pt layer would remain firmly attached to the surface. The GLAD depositions were carried out by e-gun stimulated thermal evaporation at 5° between the evaporation flux and the substrate at deposited Pt surface mass densities of 1.6×10^{-5} ($g\,cm^{-2}$), 3.2×10^{-5} ($g\,cm^{-2}$), and 6.4×10^{-5} ($g\,cm^{-2}$), using Pt with a purity of 99.9% (Pt from Dansk Aedelmetal A/S, Denmark, 99.9% purity). The deposited surface mass densities were monitored by a quartz crystal microbalance (QCM) and corrected by a cosine ($90° - \theta$) factor due to the reduced incoming flux caused by the tilted substrate plane. We defined the angle of incidence θ as the angle between the incident vapor direction and the substrate plane (see Figure 1A). The GLAD

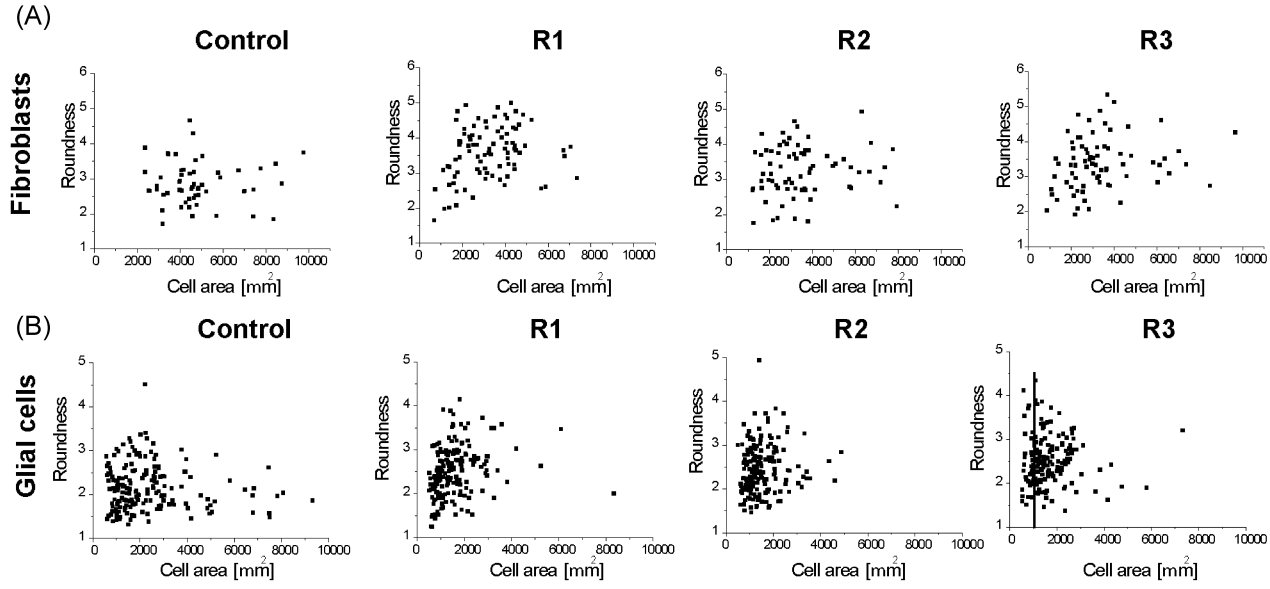

Fig. 4. Roundness versus cell area distributions for the fibroblasts (A) and glial cells (B) on the respective surfaces.

evaporation was carried out at room temperature with a background pressure $<10^{-8}$ mbar and a distance between the evaporation source and the substrate at 250 mm. During GLAD the substrates were rotated at three rotations per minute. After GLAD deposition, the samples were heated up to 160 °C for 1 h in an oven. The heating step was followed by sputter deposition of 25 nm to assure a homogenous Pt coverage. The flat Pt reference surfaces for the cell assays were produced by sputtering 100 nm Pt on a silicon wafer (Si-Mat, Germany) at room temperature with an Argon pressure of 2×10^{-3} mbar and AFM measurements confirmed a low roughness value (0.64 ± 0.004 nm).

1.2. Material Characterization

After GLAD deposition was carried out on the respective substrates images were acquired by means of AFM using a commercial Nanoscope IIIA Multimode SPM (Veeco instruments, Santa Barbara, CA). AFM images were acquired in the tapping mode at scan frequencies 1–2 Hz under ambient conditions using a silicon cantilever (NSG01, NT-MDT, Russia) with a typical resonance frequency at 150 kHz, a spring constant of 5.5 N m^{-1} and a tip radius below 10 nm. The AFM images were quadratic with a linear dimension of 2 mm and a linear resolution of 512 pixels. The AFM images were complemented with cross-section and plan-view SEM images (FEI Company, USA). These images were analyzed with ImageJ software (from www.rsbweb.nih.gov) to determine the height and width of the submicron islands (brush columns), as well as the thickness of the respective Pt coatings. The column height and width are presented in the paper as mean ± standard error of mean from a total of 15 submicron islands. No significant sample variations were seen.

1.3. Cell Culture

In brief, test samples consisted of a flat and three different nanorough surfaces attached to a microscope slide using medical-grade silicone adhesive (MED-1037, NuSil Technology, USA). Samples were cleaned by immersion in a solution 1% v/v of detergent (Liquinox, PC International Ltd, UK), rinsed with ultrapure water, and sterilized using 70% ethanol. Samples were introduced in separate cell culture dishes (35 mm BD Falcon, BD Biosciences, Broendby, Denmark) and seeded with either fibroblasts or glial cells at an approximate density of 5000 cells cm^{-2}. The culture medium consisted of Dulbecco's Modified Eagle's medium (DMEM, Invitrogen, Taastrup, Denmark) supplemented with 10% fetal calf serum, and 1% penicillin/streptomycin. The fibroblasts were obtained from a human skin biopsy, while the glial cells consisted of a human astrocytoma-derived glial cell line (U-87, ATCC no. HTB-14). After 24 h of culture on the test samples, the cells were rinsed with phosphate buffer saline (PBS), fixed with 4% buffered formaldehyde and permeabilized with 0.1% Triton X-100 in PBS for 5 min. The cell nucleus was then stained with the Hoechst 33342 dye (Molecular Probes, Carlsbad, CA, USA) for 1 h at 37 °C, rinsed with PBS and incubated with a 1:200 dilution of primary antibody anti-vinculin produced in rabbit (Sigma–Aldrich A/S, Broendby, Denmark) for 1 h at 37 °C. Samples were then rinsed in PBS and incubated in a 1:150 dilution of secondary antibody anti-rabbit Cy5-conjugated produced in goat (Invitrogen) under mild shaking for 1 h at room temperature. Finally, the actin cytoskeleton was stained by incubating the samples for 20 min in a PBS solution containing 1% bovine serum albumin (BSA) and a 1:40 diluted Bodipy 558/568 Phalloidin (Invitrogen), which binds specifically to the actin cytoskeleton. Following the cytoskeletal immunostaining, the samples were rinsed twice with PBS and kept at 4 °C in PBS until microscopic analysis.

1.4. Cell Counting and Cell Morphology

Light microscopy was performed with a Leica DM 6000B microscope, where images were acquired at random on each surface. Area, elongation, and roundness of isolated cells were analyzed with the grain analysis tool provided with the ImageJ software. Elongation indicates how elongated a shape is and is defined as Elongation = (Length – width)/(Length), while the roundness value is a measure of the irregularity of an object compared to a circle and defined as roundness = perimeter/(4π Area). The 0.5 means square root of the parenthesis.

1.5. Statistics

All data was expressed as mean ± standard error of mean. Differences between two groups were calculated by the Student's *t*-test, with significant levels of difference set at the 95, 99, and 99.9% confidence interval and marked with *($p < 0.05$), **($p < 0.01$), and ***($p < 0.001$), respectively.

Received: February 4, 2014
Final Version: March 19, 2014
Published online: May 11, 2014

[1] A. K. Gaharwar, N. A. Peppas, A. Khademhosseini, *Biotechnol. Bioeng.* **2014**, *111*, 441.
[2] A. Dolatshahi-Pirouz, M. Nikkhah, K. Kolind, M. R. Dokmeci, A. Khademhosseini, *J. Funct. Biomater.* **2014**, *2*, 88.
[3] E. S. Place, N. D. Evans, M. M. Stevens, *Nat. Mat.* **2009**, *8*, 457.
[4] T. Jensen, J. Baas, A. Dolatshahi-Pirouz, T. Jacobsen, G. Singh, J. V. Nygaard, M. Foss, J. Bechtold, C. Bünger, F. Besenbacher, K. Sùballe, *J. Biomed. Mater. Res. Part A* **2011**, *99*, 94.
[5] P. Roach, D. Farrar, C. C. Perry, *J. Am. Chem. Soc.* **2006**, *128*, 3939.
[6] R. S. Kane, A. D. Stroock, *Biotechnol. Prog.* **2007**, *12*, 316.
[7] J. Ahn, S. J. Son, J. Min, *J. Biotechnol.* **2013**, *164*, 543.
[8] C. P. Pennisi, C. Sevcencu, A. Dolatshahi-Pirouz, M. Foss, J. Lundsgaard Hansen, A. Nylandsted Larsen, V. Zachar, F. Besenbacher, K. Yoshida, *Nanotechnology* **2009**, *20*, 385103.

[9] K. Kolind, A. Dolatshahi-Pirouz, J. Lovmand, F. S. Pedersen, M. Foss, F. Besenbacer, *Biomaterials* **2010**, *31*, 9182.
[10] A. Dolatshahi-Pirouz, M. Foss, F. Besenbacher, *J. Phys. Chem. C* **2011**, *115*, 13617.
[11] O. Zinger, G. Zhao, Z. Schwartz, J. Simpson, M. Wieland, D. Landolt, B. Boyan, *Biomaterials* **2005**, *26*, 1837.
[12] A. Ranella, M. Barberoglou, S. Bakogianni, C. Fotakis, C. Stratakis, *Acta Biomater.* **2010**, *6*, 2711.
[13] G. Zhao, A. L. Raines, M. Wieland, Z. Schwartz, B. D. Boyan, *Biomaterials* **2007**, *28*, 2821.
[14] S. R. Kennedy, M. J. Brett, *J. Vac. Sci. Technol. B* **2004**, *22*, 1184.
[15] S. R. Kennedy, M. J. Brett, O. Toader, S. John, *Nano Lett.* **2002**, *2*, 59.
[16] K. Robbie, J. C. Sit, M. J. Brett, *J. Vac. Sci. Technol. B* **1998**, *B 16*, 1115.
[17] A. Dolatshahi-Pirouz, C. P. Pennisi, S. Skeldal, M. Foss, J. Chevallier, V. Zachar, P. Andreasen, K. Yoshida, F. Besenbacher, *Nanotechnology* **2009**, *20*, 095101.
[18] A. Dolatshahi-Pirouz, S. Skeldal, M. B. Hovgaard, T. Jensen, M. Foss, J. Chevallier, F. Besenbacher, *J. Phys. Chem. C* **2009**, *113*, 4406.
[19] A. Dolatshahi-Pirouz, K. Rechendorff, M. B. Hovgaard, M. Foss, J. Chevallier, F. Besenbacher, *Colloids Surf. B* **2008**, *66*, 53.
[20] K. Rechendorff, M. B. Hovgaard, J. Chevallier, M. Foss, F. Besenbacher, *Appl. Phys. Lett.* **2005**, *87*, 073105.
[21] A. Dolatshahi-Pirouz, M. B. Hovgaard, K. Rechendorff, J. Chevallier, M. Foss, F. Besenbacher, *Phys. Rev. B* **2008**, *B 77*, 115427.
[22] A. Dolatshahi-Pirouz, D. S. Sutherland, M. Foss, F. Besenbacher, *Appl. Surf. Sci.* **2011**, *257*, 2226.
[23] J. R. Frederick, J. D'Arcy-Gall, D. Gall, *Thin Solid Films* **2006**, *494*, 330.
[24] J. R. Frederick, D. Gall, *Appl. Phys. Lett.* **2005**, *87*, 053107.
[25] C. Zhou, D. Gall, *J. Vac. Sci. Technol. A* **2007**, *25*, 312.
[26] C. M. Zhou, D. Gall, *Thin Solid Films* **2006**, *515*, 1223.
[27] A. Dolatshahi-Pirouz, T. Jensen, T. V. Jensen, R. Bech, J. Chevallier, F. Besenbacher, M. Foss, D. S. Sutherland, *Adv. Eng. Mater.* **2010**, *12*, 899.
[28] W. M. Grill, S. E. Norman, R. V. Bellamkonda, *Annu. Rev. Biomed. Eng. Annu. Rev.* **2009**, *11*, 24.
[29] A. D. Bershadsky, I. S. Tint, A. A. Neyfakh, J. M. Vasiliev, *Exp. Cell Res.* **1985**, *158*, 433.
[30] K. M. Yamada, B. Geiger, *Curr. Opin. Cell Biol.* **1997**, *9*, 76.
[31] A. E. Aplin, A. Howe, R. L. Juliano, *Curr. Opin. Cell Biol.* **1999**, *11*, 737.
[32] E. Ruoslahti, B. Obrink, *Exp. Cell Res.* **1996**, *227*, 1.
[33] C. S. Chen, M. Mrksich, S. Huang, G. M. Whitesides, D. E. Ingber, *Science* **1997**, *276*, 142.
[34] T. Jensen, et al. *Colloids Surf. B* **2010**, *75*, 186.
[35] P. T. de Oliveira, A. Nanci, *Biomaterials* **2004**, *25*, 403.
[36] A. Dolatshahi-Pirouz, et al. *Colloids Surf. B* **2010**, *84*, 18.
[37] K. Burridge, M. Chrzanowska-Wodnicka, *Annu. Rev. Cell Dev. Biol.* **1996**, *12*, 463.

